Hot Ductility Behavior and Repair Weldability of Service-Aged, Heat-Resistant Stainless Steel Castings

Significant differences in hot ductility behavior and repair weldability were observed among Nb-bearing stainless steel castings after exposure to similar service conditions

BY S. SHI, J. C. LIPPOLD, AND J. RAMIREZ

ABSTRACT

The loss of repair weldability after service exposure in heat-resistant alloys has been related to the loss of ductility due to the formation of carbides and other compounds, such as nickel silicide. The hot ductility behavior of three service-aged, heat-resistant stainless steel castings, HP-45Nb, HP-50Nb, and 20-32Nb, were studied using the Gleeble® thermomechanical simulator. Results from hot ductility testing are presented and detailed fractographic analysis of samples tested at 900° and 1100°C is described. During the simulated cooling cycle, the HP-Nb modified alloy demonstrated significantly higher ductility as compared to the 20-32Nb alloy. The differences in high-temperature stability of the preexisting embrittling constituents in these alloys resulted in different microstructure evolution that influenced their hot ductility behavior. Based on the results, the service-exposed HP-Nb modified alloy is considered to have acceptable repair weldability. In contrast, the service-exposed 20-32Nb alloys showed severe susceptibility to liquation cracking and significant loss in on-cooling ductility, and are considered difficult to repair unless a high-temperature solution annealing heat treatment is performed.

Introduction

Heat-resistant, cast stainless steels such as Alloy HP-Nb modified (ASTM A297) and Alloy 20-32Nb (ASTM A351/A351M-05) are used in applications requiring good corrosion resistance and moderate strength at temperatures up to 1100°C (2012°F) (Ref. 1). At these temperatures the cast microstructure will transform with time leading to the formation of carbides and other compounds, such as nickel silicide. The loss of repair weldability after service exposure in these heat-resistant alloys, including HP-Nb modified and 20-32Nb, has been related to the loss of ductility due to the formation of $M_{23}C_6$ and nickel silicide (Refs. 2–4). Cracking during shut-down or repair welding due to the service-induced embrittlement of these heat-resistant castings is of great practical concern in the power-generation, refinery, and petrochemical industries. The materials studied were provided by two independent petrochemical companies. The as-received HP-45Nb has experienced fracture during service — Fig. 1. For the 20-32Nb alloy, liquation cracking was immediately observed in the heat-affected zone (HAZ) during repair welding — Fig. 2. Difficulties in repair of service-exposed 20-32Nb alloy have been reported in other refineries. As shown in Fig. 3, cracking has been observed during repair welding. One of the objectives of this work was to develop a fundamental understanding of the repair weldability of the three materials provided.

Microstructure evolution during service exposure and simulated thermal exposure during repair are critical to understanding the hot-ductility behavior discrepancies and resultant repair weldability between the two types of alloys. Microstructure evolution in these materials from the as-cast condition to the service-exposed condition is described elsewhere (Ref. 5). It was found that the atomic ratio of Nb to C is a key factor in determining the type of carbides formed during service exposure. The microstructure evolution process is summarized in Table 3 of Ref. 5.

In this investigation, the Gleeble®, a programmable thermal-mechanical simulator, was used to study the hot ductility behavior of service-exposed HP-Nb modified and 20-32Nb alloys during simulated repair welding thermal cycles. The implications on repair weldability are discussed.

KEYWORDS

Hot Ductility Test
Cast Stainless Steels
Heat-Resistant Stainless Steels
Weldability
Nb-Bearing Stainless Steels
Gleeble®
Repair Weldability

Materials and Experimental Procedures

Materials. Heat-resistant HP-Nb modified (for simplicity, they are referred to here as HP-Nb alloys) and 20-32Nb alloys are the most commonly used cast high-temperature furnace tube alloys. The specification of HP-Nb alloys is described in ASTM A297 (Ref. 6); and the 20-32Nb alloy is covered under ASTM A351/A351M-05 (Ref. 7), but are usually identified by their trade names such as KHR32C (Ref. 8) and CR32W (Ref. 9). The compositions of the alloys evaluated in this study are provided in Table 1. The number of years of service exposure at approximately 815°C (1500°F) is also indicated in the table.

Characterization. Microstructure

S. SHI (shu.shi@shell.com) *is welding and materials specialist, Shell Global Solutions, Houston, Tex. J. C. LIPPOLD* (lippold.1@osu.edu) *is professor, Welding Engineering Program, The Ohio State University, Columbus, Ohio. J. RAMIREZ is principal engineer, Edison Welding Institute, Columbus, Ohio.*

Fig. 1 — As-received service-exposed HP45Nb pipe section that ruptured.

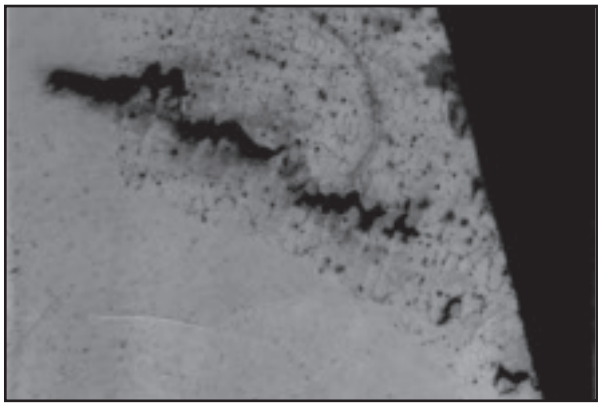

Fig. 2 — Liquation cracking observed in the HAZ of service-exposed 20-32Nb alloy upon repair welding (750×). (Photo courtesy of Syncrude Canada Ltd.)

characterization was performed on both service-exposed (EX) and simulated as-cast alloys (CA). Due to the difficulty in obtaining unexposed, as-cast material of similar composition, the EX alloys were remelted using a button melting apparatus to simulate the original as-cast microstructure. The button melting apparatus uses a tungsten torch with argon shielding to produce small cast samples.

The methods used for microstructure characterization and fractographic analysis included optical microscopy (OM) and scanning electron microscopy (SEM). SEM analysis was conducted in both the secondary electron (SE) and backscattered electron (BSE) modes. Composition analysis and line scan analysis were conducted using both Philips XL-30 ESEM FEG and FEI Sirion FEG[1] microscopes equipped with X-ray energy-dispersive spectroscopy (XEDS). With the combination of SE, BSE, and EDS analysis, it is possible to make reasonable estimates of the precipitates and intermetallic phases that are present.

Hot Ductility Testing. Hot ductility behavior was studied using the Gleeble® 3800, which has been used extensively for studying the weldability of a wide variety of materials (Refs. 10–19). Hot ductility tests are essentially high-temperature tensile tests, but are conducted both "on-heating" and "on-cooling." The test technique can provide the tensile properties of the HAZ microstructure during the weld thermal cycle. Therefore, it is considered an effective method to study the nature of HAZ cracking that occurs during welding or subsequent postweld processing (Refs. 19–22).

In this study, the hot ductility of each of the materials was determined by both on-heating and on-cooling tests, where the on-cooling behavior was determined after heating to a peak temperature (T_p) between the nil ductility temperature (NDT) and nil strength temperature (NST). Ductility is normally measured as the percentage of reduction of area (ROA) at a specific temperature. NDT and NST are two important points on the on-heating ductility curve. The ductility recovery temperature (DRT), the temperature at which some ductility is measured during cooling from T_p, is an important parameter during the on-cooling cycle.

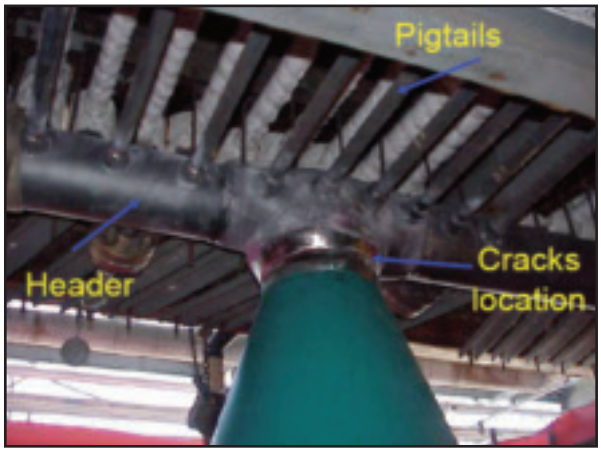

Fig. 3 — Cracking observed during repair welding of the service-exposed 20-32Nb header assembly. (Photo courtesy of Jorge Penso & Hearl Mead.)

For hot ductility testing, a test temperature and stroke (extension rate) are pre-programmed as shown schematically in Fig. 4. For on-heating tests, specimens are first heated up to the programmed temperature and held for 0.5 s to stabilize the temperature in the specimen. A stroke is then applied at the rate of 25 mm/s to pull the specimen to failure. For on-cooling tests, a peak temperature (T_p) needs to be determined. The T_p employed in hot ductility tests may be any temperature below the bulk melting temperature of the material being studied. However, T_p is normally chosen based on the tested NST. In this investigation, a temperature between NST and NST–10°C was used as T_p for on-cooling tests.

Standard hot ductility samples were used in this investigation, as shown in Fig.

Table 1 — Chemical Composition (wt-%) of Alloys Studied

ID wt-%	HP45Nb 9 year	HP50Nb 12 year	20-32Nb 3 year	20-32Nb 7 year	20-32Nb 15 year
C	0.41	0.38	0.09	0.1	0.1
Mn	1.04	1.22	1.01	0.96	1.13
P	0.022	0.031	0.013	0.014	0.013
S	0.007	0.016	0.007	0.006	0.006
Si	1.15	1.56	0.91	0.87	0.95
Cu	0.026	0.1	0.05	0.05	0.05
Mo	0.026	0.085	0.01	0.02	0.02
Ni	33.55	33.67	33.6	33.4	33
Cr	25.58	25.11	19.9	19.9	20.2
Nb	0.9	1.37	1.36	1.33	1.19
Fe	Bal	Bal	Bal	Bal	Bal

1. Philips is a trademark of Royal Philips Electronics N.V, The Netherlands. FEI and Sirion are trademarks of FEI Co., Hillsboro-Oregon, U.S.A.

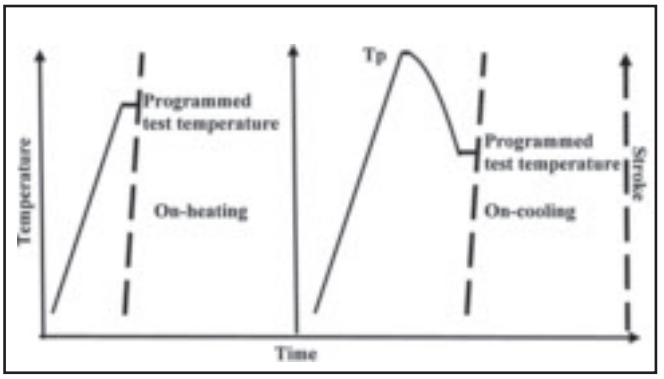

Fig. 4 — Schematic of on-heating and on-cooling hot ductility test program.

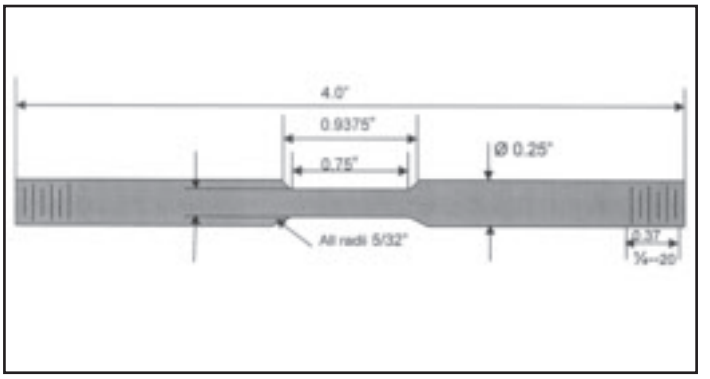

Fig. 5 — Specimen dimensions of ¼-in. round bars with reduced gauge section used in hot ductility tests of HP alloys.

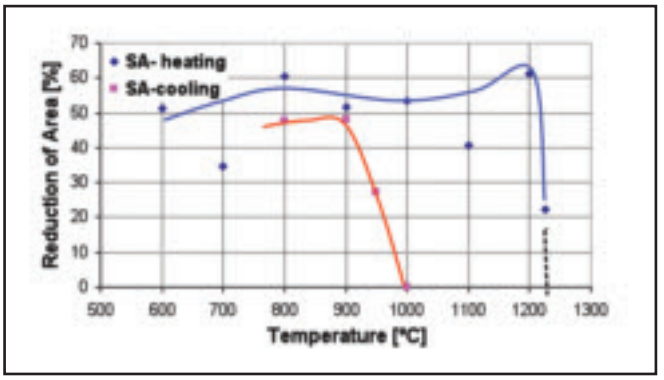

Fig. 6 — Hot ductility curves of solutionized 20-32Nb alloy.

5. Since some of the single thermal cycle hot ductility tests were conducted at relatively low temperatures, specimens with a reduced section at the mid-span were used to ensure that the sample would fail at the programmed temperature and at the preferred location. To prevent contamination of the fracture surface by high-temperature oxidation, tests were run in an argon atmosphere. The chamber was evacuated and backpurged twice with argon to prevent sample oxidation during testing.

To study material susceptibility to both ductility dip cracking and liquation cracking, standard hot ductility tests were performed over the temperature range from 500°C to the NST. The testing conditions are listed in Table 2.

Results and Discussion

Gleeble Hot Ductility Test Results

In this study, the temperature differential between NST and DRT (NST-DRT) is used to quantify the degree of liquation cracking susceptibility as this is the temperature range in which continuous liquid networks are present in the microstructure (Refs. 23–26). The larger the NST-DRT temperature range, the greater is the liquation cracking susceptibility. The important temperatures determined by hot ductility testing are summarized in Table 3. The NDT for the solutionized 20-32Nb alloy was not obtained due to the limited supply of material.

As Table 3 implies, the service-exposed HP alloys are relatively resistant to HAZ liquation cracking as the (NST-DRT) range is less than 20°C. In contrast, the service-exposed 20-32Nb alloys had a (NST-DRT) ranging from 86° to 209°C, indicating a greater susceptibility to HAZ liquation cracking. Solution heat treatment at 1150°C for 6 h improved the overall hot ductility (Fig. 6), but increased susceptibility to HAZ liquation cracking as the NST-DRT increased from 86° to 260°C for the 15-year service-exposed 20-32Nb alloy.

The 20-32Nb alloys have lower carbon content (~0.1 wt-%), and a lower fraction of embrittling phases, than the higher carbon HP alloys (~0.4 wt-% C). For the service-exposed condition, the embrittling phases have been reported as Ni-Nb silicide and Cr-rich, $M_{23}C_6$ for both types of alloys (Refs. 3, 5). Based on carbon content, one might expect that the 20-32Nb alloys would have better ductility than the HP alloys. The hot ductility tests, however, showed results to the contrary. As shown in Fig. 7, the on-cooling ductility for the 20-32Nb alloy from 1000° down to 600°C is less than 10%, while the ductility of the HP-Nb alloys in this same temperature range is between 10 and 20%.

The low on-cooling ductility observed in service-aged 20-32Nb alloys is related to the microstructure evolution during the service exposure and subsequent simulated on-heating and on-cooling thermal cycles. The microstructure during service exposure is discussed in detail elsewhere (Ref. 5). The microstructure changes dur-

Table 2 — Parameters Used in Hot Ductility Tests

Parameters	Value
Heating rate	100°C/s
Holding time at test temperature	0.5 s
Holding time at peak temperature	0.05 s
Applied stroke rate	25 mm/s
Cooling rate for peak temperature	Free cooling (50 to 25°C/s)

Table 3 — Important Temperatures (°C) Obtained from the Gleeble Hot Ductility Tests

	Service-exposed HP alloys		20-32Nb alloys			
	HP45Nb	HP50-Nb	3 year	7 year	15 year	Solutionized
T_p	1240	1170	1200	1210	1190	1250
NST	1250	1177	1209	1218	1196	1260
NDT	1236	1171	1159	1162	1151	—
DRT	1232	1163	1088	1009	1110	1000
NST-DRT	18	14	121	209	86	260

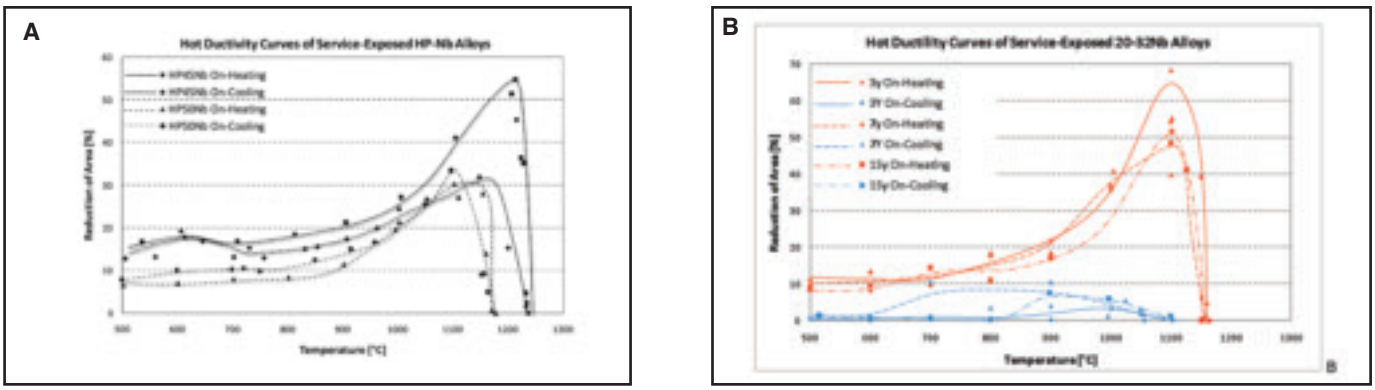

Fig. 7 — Hot ductility curves of service-exposed alloys: A — HP-Nb; B — 20-32Nb.

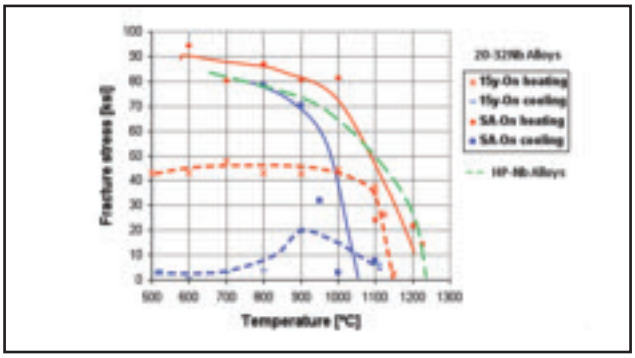

Fig. 8 — Results of fracture stress obtained with Gleeble hot ductility tests. The green line represents the HP-Nb fracture stress behavior.

ing simulated on-heating and on-cooling cycles are discussed later in this paper.

Fracture stress is a material property, and is defined as the true, normal stress on the minimum cross-sectional area at the beginning of fracture (Ref. 29). Therefore, a material with a higher fracture stress can tolerate more restraint, which can be a form of heat shrinkage stress or any external applied stress during cooling. In the hot ductility tests, the dynamic loads were recorded by the data acquisition system. The maximum load at the test temperature indicated the beginning of fracture, since the load starts to drop once the facture occurs. The fracture stresses at different test temperatures were calculated using the following equation:

$$Fracture\ Stress = \frac{F_{max}}{A_f}$$

where F_{max} is the maximum load recorded, and A_f is the cross-sectional area at the fracture surface.

The calculated fracture stresses vs. temperatures are plotted in Fig. 8. For the HP alloys, the fracture stress showed a similar trend of decreasing as the temperature increased on both heating and cooling tests. No degradation of fracture stress was observed during the on-cooling cycle. A green dotted line is used to represent the fracture stress behavior of the HP-Nb alloys.

In contrast, all three service-exposed 20-32Nb alloys exhibited a much lower fracture stress over the entire test temperature range as compared to the HP-Nb alloys. For instance, at 900°C during the on-cooling test, the fracture stress obtained was 70 ksi for the HP-Nb alloys, but only 20 ksi for the 20-32Nb alloys. In the on-heating tests, the fracture stress remained relatively constant until the temperature reached 1100°C. Above 1100°C, the fracture stress decreased dramatically. This agrees with the on-heating hot ductility behavior observed: above 1100°C, the ductility suddenly dropped from more than 40% to 0% for the 20-32Nb alloys. A significant loss in fracture stress was observed in the on-cooling tests. Since all three 20-32Nb alloys exhibited similar trends in fracture stress, only the 15-year alloy was plotted. One red dotted line and one blue dotted line were used to simplify the trend of fracture stress on-heating and on-cooling of the service-exposed 20-32Nb alloys, respectively. The solutionized 20-32Nb alloy exhibited a comparable fracture stress to the service-exposed HP-Nb alloys, which implies similar fracture resistance between the service-exposed HP-Nb alloy and 20-32Nb alloy prior to service exposure.

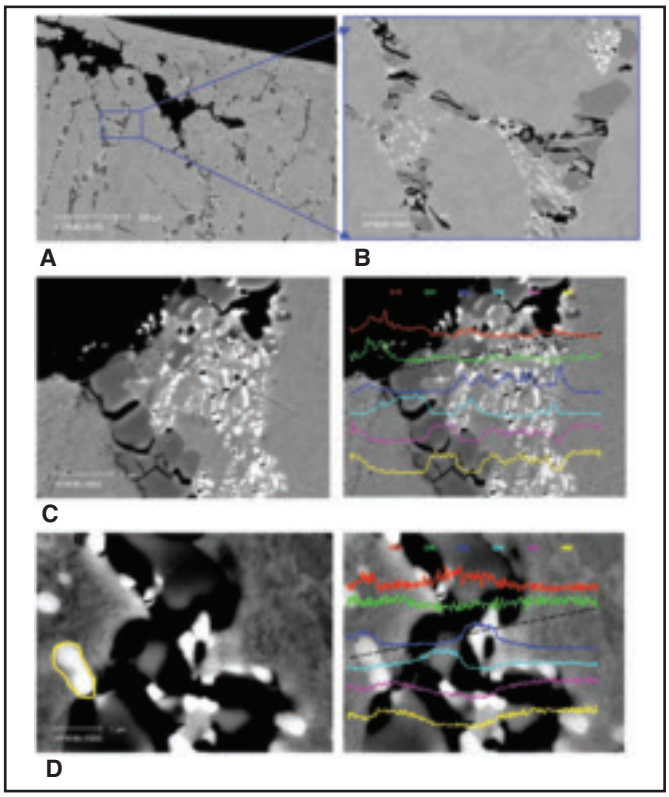

Fig. 9 — Fracture profile of HP45Nb Gleeble sample tested at 900°C on heating: A — Overall view; B — microcracking in Cr-rich particles; C — EDS line scan at dark phase showed a high Cr concentration; D — EDS line scan at bright phase showed a high Nb concentration.

Fractographic Analysis

Changes in material mechanical properties, in general, are associated with a microstructural change. The loss of on-cooling ductility and fracture stress of the 20-32Nb alloys was believed to be due to the microstructure evolution that occurred at elevated temperatures. To study the

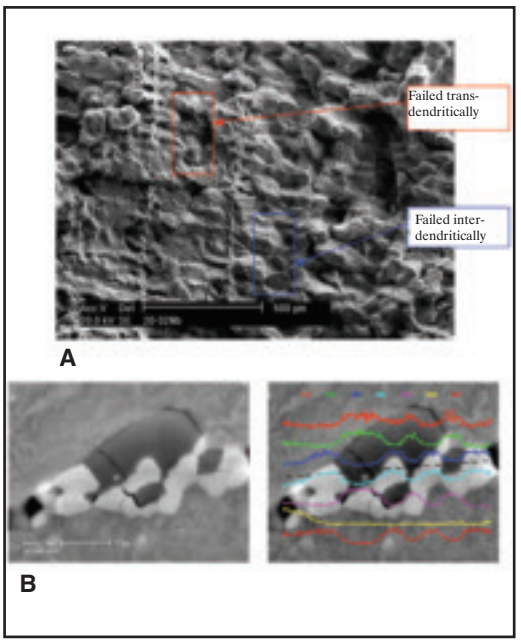

Fig. 10 — Fracture surface of service-exposed 20-32Nb sample tested at 900°C on heating: A — Fracture mode viewed at low magnification; B — EDS line scan results of the $M_{23}C_6$ and Ni-Nb silicide.

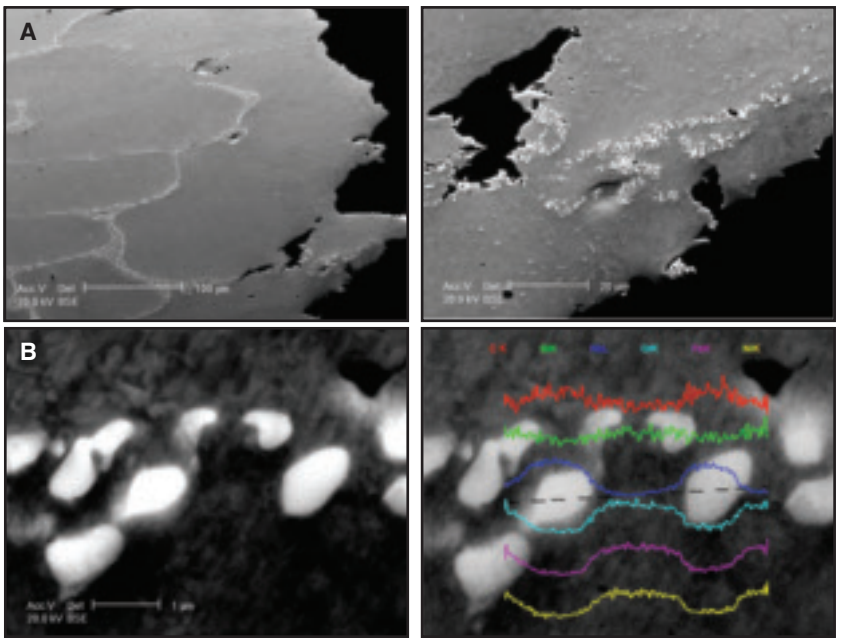

Fig. 11 — Fracture profile of solutionized 20-32Nb sample tested at 900°C on heating: A — Deformed dendritic structure; B — EDS line scan result.

cause of variations in ductility and fracture stress in these materials, hot ductility samples tested at 900° and 1100°C on both on-heating and on-cooling were subjected to fractographic analysis in the SEM. EDS spot and line scan techniques were used extensively to analyze the microconstituents on the fracture surface or in the microstructure. All the metallographically polished samples were examined in the unetched condition. The backscattered electron (BSE) detector in the SEM was used to provide phase contrast.

The two service-exposed HP alloys under investigation showed similar results regarding the ductility and fracture stress. The HP45Nb alloy was chosen for the fractographic analysis. The hot ductility results for the service-exposed 20-32Nb alloys are essentially the same regardless of the service exposure times.

On-heating at 900°C. When tested at 900°C on-heating, both Cr-rich and Nb-rich particles were found in the service-exposed HP-Nb and 20-32Nb alloys (Figs. 9, 10). In the HP alloy, evidence of transformation from Ni-Nb silicide to NbC was also observed. In contrast, no such evidence was found in the service-exposed 20-32Nb alloys. This may be due to the higher carbon concentration in the HP-Nb alloys, which promoted a higher fraction of $M_{23}C_6$ formation during service. When the alloy was heated to 900°C, $M_{23}C_6$ started to dissolve, putting carbon back into solution. The free carbon in solution promoted the decomposition of Ni-Nb silicide due to a high affinity between niobium and carbon. Because the transformation requires carbon diffusion from dissolved $M_{23}C_6$ to Ni-Nb silicide, the transformation is limited under fast heating conditions. In the 20-32Nb alloy, this type of reaction is further retarded because of a relatively small amount of $M_{23}C_6$ and a large dendrite size. The result is that the carbon content is not sufficient and/or the diffusion distances are not short enough to trigger the transformation from Ni-Nb silicide to NbC at a temperature of 900°C.

Only Nb-carbides existed in the solutionized 20-32Nb alloy — Fig. 11. Small cracks were associated with particles of the service-exposed alloys, and large cavities formed at the triple-point grain boundary junctions in the solutionized alloy.

On-heating at 1100°C. Nb-carbides were observed on the fracture surface of all samples when tested at 1100°C on heating. In contrast, no Nb-carbides were found in the service-exposed 20-32Nb alloy when tested at 900°C on heating. This indicated that the transformation from Ni-Nb silicide to NbC occurred at a higher temperature in the 20-32Nb alloy as compared to the HP-Nb alloy. In the service-exposed HP alloy, the $M_{23}C_6$ carbide and Ni-Nb silicide no longer existed at the fracture area. In contrast, $M_{23}C_6$ and Ni-Nb silicide were found in the service-exposed 20-32Nb alloy. NbC is the only phase that was present in the solutionized 20-32Nb alloy.

On-cooling at 1100°C. As compared to samples tested at 1100°C on heating, no significant changes regarding the type and morphology of constituents were found at the fracture area of the service-exposed HP alloy and solutionized 20-32Nb alloy when samples were tested at 1100°C on cooling. For the service-exposed 20-32Nb alloy, apparent liquation was observed around the Nb-rich particles (Fig. 12), which can be fully transformed NbC or a partially transformed component from Ni-Nb silicide. The high concentration of silicon around the particle (Fig. 13) increases the susceptibility to liquation. Once the liquation formed continuously around the dendrite boundary, a significant loss in on-cooling ductility of the alloy would be expected.

On-cooling at 900°C. At the on-cooling test temperature of 900°C, transformation from Ni-Nb silicide to Nb-carbides was observed in both service-exposed HP-Nb alloy and 20-32Nb alloy. Chromium-rich particles were observed in the HP-Nb alloy, but not in any of the other materials. Recrystallization occurred in the service-exposed 20-32Nb alloy — Fig. 14. No liquation was found in the HP alloy but liquation was evident in the service-exposed 20-32Nb alloy. Niobium-carbides were the only constituent

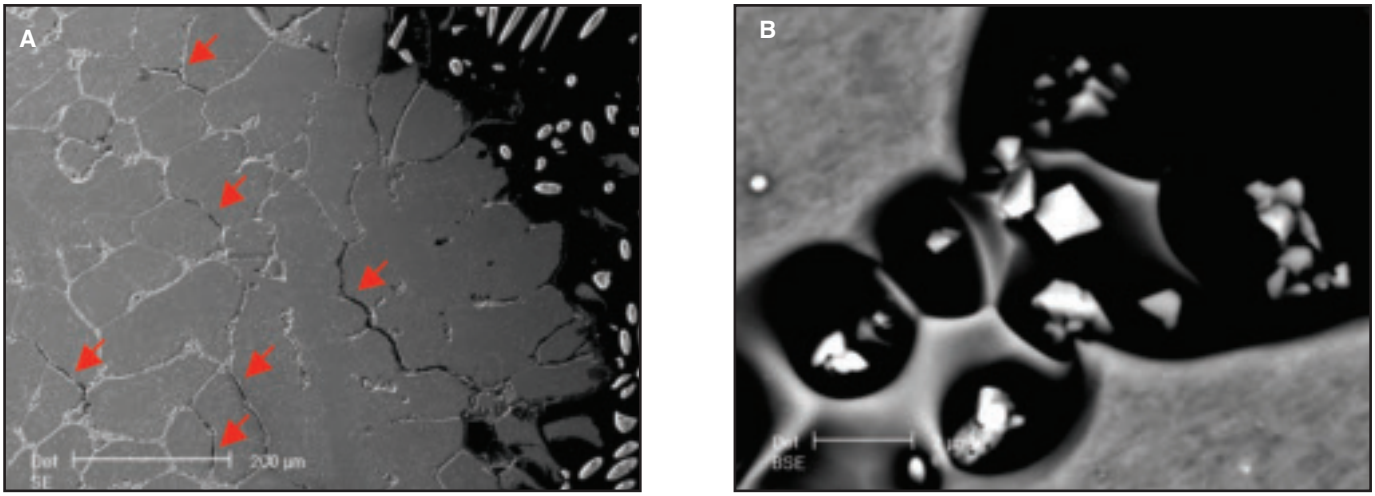

Fig. 12 — Fracture profile of service-exposed 20-32Nb sample tested at 1100°C on cooling: A — Interdendritic failure; B — liquation around Nb-rich particle.

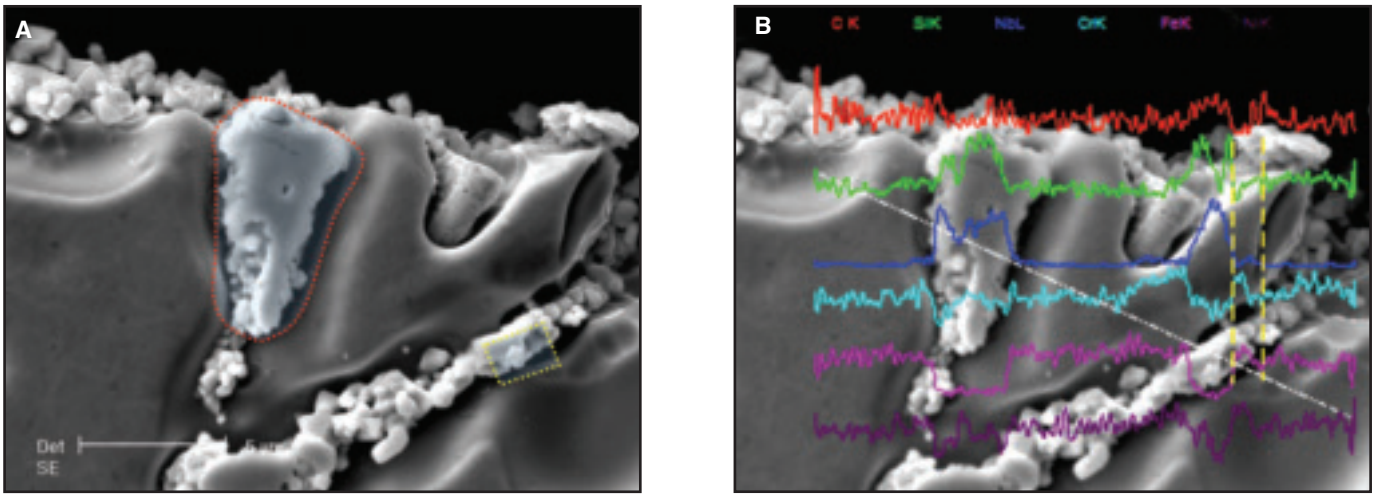

Fig. 13 — EDS results of the particles presented at the fracture area of 20-32Nb sample tested at 1100°C on cooling: A — EDS spot scan result from a square-shaped particle; B — EDS line scan results.

present in the solutionized alloy.

Transformation from Ni-Nb Silicide to NbC

The transformation behavior was studied using the SEM/EDS spot analysis and line scan technique. The spot analysis results revealed the particle (Fig. 15A) is rich in Si, Nb, and Ni, and can be characterized as Ni-Nb silicide. The dark lines in the pictures represent the position that has been analyzed due to "charging" of the sample by the electron beam. Nickel content has dropped to approximately the nominal composition. No carbon was detected in this particle. This is because the Cr-rich, $M_{23}C_6$ is of relatively low concentration in the alloy, and at this stage the concentration of carbon from the dissolution of the $M_{23}C_6$ is not high enough to be detected by the SEM. This signified the initial stage of the transformation from Ni-Nb silicide to Nb-carbide.

A further transformation can be illustrated with Fig. 15B. Peaks in carbon and silicon were observed at the edge of the white particle. Within the particle, the Ni concentration dropped well below that of the matrix, but the Nb concentration still remained high. It is most likely that the formation of NbC would start at the edge of the original Ni-Nb silicide due to a high concentration of carbon. The observed transformation in Fig. 15B presents the second stage of the transformation from Ni-Nb silicide to NbC. In Fig. 15C, particles on the left side of the picture showed enrichment in carbon and niobium and depletion in Ni, Cr, and Fe, representing a complete transformation to NbC. The newly formed Nb-carbides are much smaller than the Ni-Nb silicide. It is likely that a Ni-Nb silicide particle would break down into several NbC particles as a consequence of the transformation. A high Si concentration was also expected around the transformed NbC, and is confirmed in Fig. 15C. As highlighted by a red circle, a peak in silicon was observed at the region between two NbC particles.

The phenomenon involving diffusion of Si and Ni to NbC during aging was previously studied by Patchett (Ref. 3). The transformation from Ni-Nb silicide to NbC during a simulated thermal cycle is the reverse reaction from the aging process as the thermal-dynamic condition favors the formation of NbC at higher temperature.

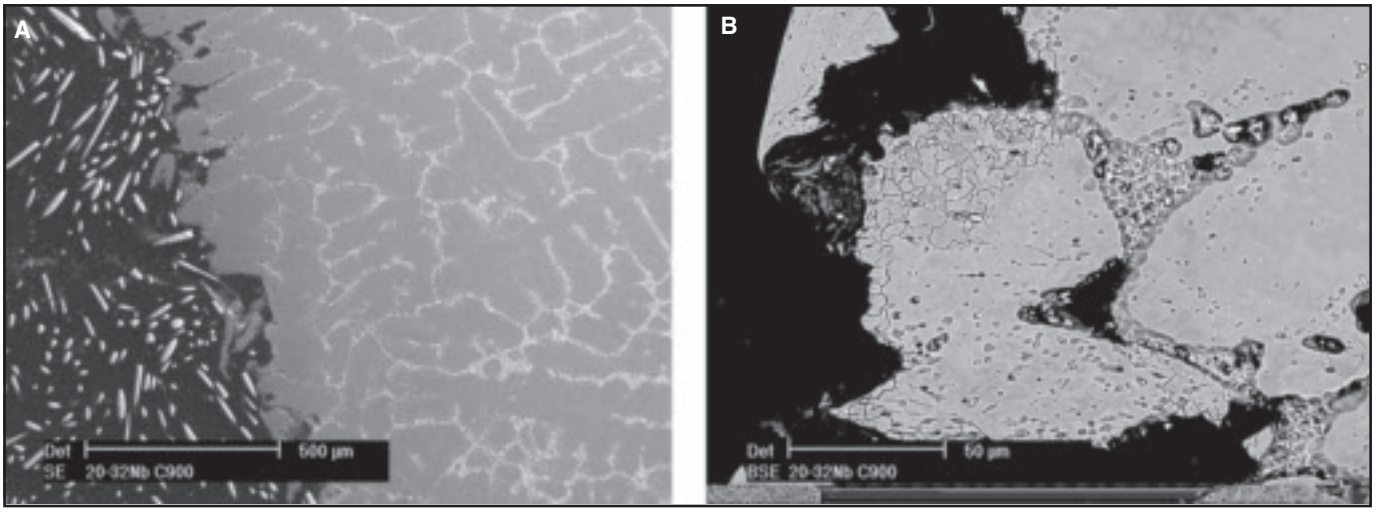

Fig. 14 — Fracture profile of service-exposed 20-32Nb sample tested at 900°C on cooling: A — Interdendritic fracture profile; B — recrystallization at dendrites along the fracture path.

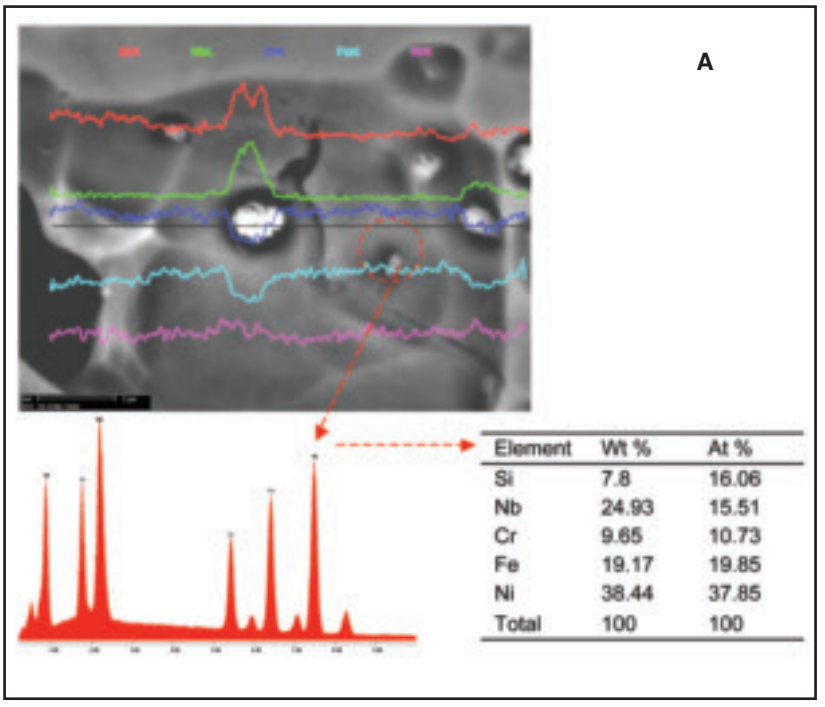

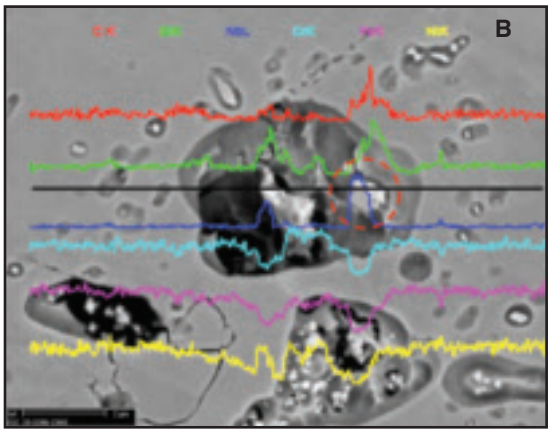

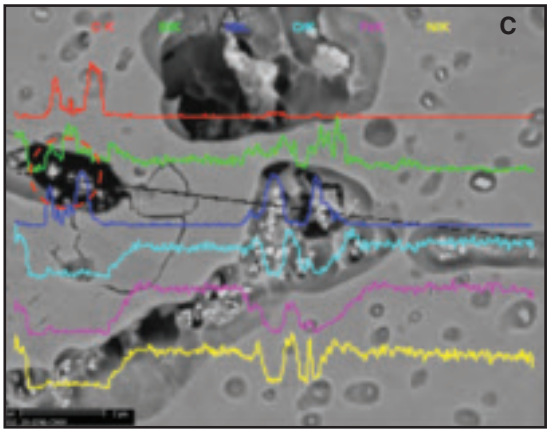

Fig. 15 — EDS result of the process of transformation from Ni-Nb silicide to NbC carbide: A —Ni-Nb silicide; B — the transient component from Ni-Nb silicide; C — NbC.

Repair Weldability

The service-exposed HP-Nb alloys exhibited good metallurgical stability, fracture stress, and on-cooling ductility, which could be related to acceptable repair weldability of this alloy. Reasonable repair weldability of service-aged HP-Nb alloy is also reported elsewhere (Ref. 27). In contrast, service-exposed 20-32Nb alloys showed severe susceptibility to liquation cracking and significant loss in on-cooling ductility and fracture stress. The susceptibility to liquation cracking was related to the combined effect of a high silicon concentration at the dendrite boundaries resulting from the dissolution of Ni-Nb silicide, and a NbC constitutional liquation mechanism. The loss in on-cooling ductility that resulted from these two mechanisms persisted from the peak HAZ temperatures of nearly 1300°C to below 900°C. After solution annealing at 1150°C for 6 h, the on-cooling hot ductility and the fracture stress of the 20-32Nb alloy was restored, but with an increase in liquation cracking susceptibility at high temperatures as the (NST-DRT) range increased to 260°C. This indicates that the extent of the HAZ in the 20-32Nb alloy exposed to the (NST-DRT) range must be minimized by increasing the temperature gradient in the HAZ during repair welding. This is

probably best achieved with low heat input practice (Ref. 28).

Summary

This paper presents the results of hot ductility testing of heat-resistant austenitic stainless steels, HP-Nb and 20-32Nb, that had experienced extended service exposure at 815°C (1500°F). Detailed metallographic and fractographic analyses were performed on hot ductility samples tested at 900° and 1100°C, both on-heating to the NDT temperature and on-cooling from a temperature slightly below the NST.

The hot ductility tests revealed that the HP-Nb alloys had much better ductility and higher fracture stress than the 20-32Nb alloys over the entire range of test temperatures. No significant loss in either ductility or fracture stress occurred in the HP-Nb alloys during the on-cooling tests. The HP-Nb alloys also exhibited a narrow range between NST and DRT (less than 20°C), indicating good resistance to liquation cracking. In contrast, a significant degradation in both ductility and fracture stress was observed in the service-exposed 20-32Nb alloys during the on-cooling tests. The service-exposed 20-32Nb alloys are expected to have a high susceptibility to liquation cracking resulting from a large range between NST and DRT (up to 200°C). Recovery in overall ductility and fracture stress was observed only when the service-exposed 20-32Nb alloy was resolutionized, but this was accompanied by increased susceptibility to liquation cracking.

Fractographic analysis revealed that Cr-rich and Nb-rich particles coexisted in the fracture region of all the service-exposed HP45-Nb alloy specimens. Evidence of transformation from Ni-Nb silicide to NbC was also observed. No evidence of liquation was observed in the HP45-Nb samples. In contrast, Cr-rich and Nb-rich phases coexisted only in the on-heating specimens of the service-exposed 20-32Nb alloy with only a Nb-rich phase present in the on-cooling samples. This indicated that the Cr-rich phase dissolved completely in the service-exposed 20-32Nb alloy at on-heating test temperatures above 1100°C. A significant amount of liquation was observed in the on-cooling 20-32Nb samples, which was a direct result of the high concentration of silicon in the microstructure. The high concentration of silicon was the by-product of the transformation from Ni-Nb silicide to NbC, which decreased the local melting temperature significantly, leading to low on-cooling ductility by liquation at temperatures down to 1100°C.

The distinct difference in the hot ductility behavior and microstructure evolution during the simulated HAZ thermal cycle between the HP-Nb alloys and the 20-32Nb alloys indicates that service-exposed HP-Nb alloys have acceptable repair weldability and service-exposed 20-32Nb may be very difficult to repair unless a solution annealing heat treatment is performed.

Acknowledgments

This investigation was supported by the Research Members of the Edison Welding Institute through the EWI Cooperative Research Program. The material used in this study was provided by Syncrude in Alberta, Canada, and ExxonMobil.

References

1. Centralloy 4852 (HP+Nb) Alloy Digest, Filling code: SS-609, Sept. 1995.

2. Haro, S. R. 2000. Microstructural factors that determine the weldability of a high Cr-high Si HK40 alloy. *Materials Chemistry and Physics* (66): 90–96.

3. Patchett, B. M., and Skwarok, R. W. 1998. Welding metallurgy of 20Cr-32Ni-Nb and HP 45 casting. *Materials for Resource Recovery and Transport.* Ed. L. Collins, pp. 379–390. Metallurgical Society of CIM.

4. Nishimoto, K., Saida, K., Inui, M., and Takahashi, M. 2001. Mechanism of hot cracking in the heat-affected zone of repair welds. Repair weld cracking of service-exposed HP-modified heat-resisting cast alloys (3rd Report). *Welding International* 15(9): 699–708.

5. Shi, S., and Lippold, J. C. 2008. Microstructure evolution during service exposure of two cast, heat-resisting stainless steels — HP-Nb modified and 20-32Nb alloys. *Materials Characterization* 59(8): 1029–1040.

6. ASTM A297/A297M-08a, *Standard Specification for Steel Castings, Iron-Chromium and Iron-Chromium-Nickel, Heat Resistant, for General Application.*

7. ASTM A351/A351M-10, *Standard Specification for Castings, Austenitic, for Pressure-Containing Parts*.

8. Kubota Alloy KHR32C (heat-resistant alloy), *Alloy Digest* (USA), June 1999, SS-746, p. 2.

9. Paralloy CR32W, *Alloy Digest* (USA), Feb. 1995, SS-580, p. 2.

10. Nippes, E. F., Savage, W. F., Bastian, B. J., Mason, H. F., and Curran, R. M. 1955. Investigation of the hot ductility of high-temperature alloys. *Welding Journal* 34(4): 183.

11. Dix, A. W., and Savage, W. F. 1971. Factors influencing strain-age cracking in Inconel X-750. *Welding Journal* 50(6): 247-s to 252-s.

12. Lundin, C. D., Qiao, C. Y. P., Gill, T. P. S., and Goodwin, G. W. 1993. Hot ductility and hot cracking behavior of modified 316 stainless steel designed for high-temperature service. *Welding Journal* 72(5): 189-s to 200-s.

13. David, S. A., Horton, J. A., Goodwin, G. M., Phillips, D. H., and Reed, R. W. 1990. Weldability and microstructure of a titanium aluminide. *Welding Journal* 69(4): 133–140.

14. Damkroger, B. K., Edwards, G. R., and Rath, B. B. 1989. Investigation of subsolidus weld cracking in alpha-beta titanium alloys. *Welding Journal* 68(7): 290–302.

15. Lee, C. H., Menon, R., and Lundin, C. D. 1988. Hot ductility and weldability of free machining austenitic stainless steel. *Welding Journal* 68(6): 119-s to 130-s.

16. Lundin, C. D., Lee, C. H., and Menon, R. 1988. Weldability evaluations of modified 316 and 347 austenitic stainless steels: Part 1 — Preliminary results. *Welding Journal* 67(2): 35-s to 46-s.

17. Norton, S. J., and Lippold, J. C. 2003. Development of a Gleeble-based test for post-weld heat treatment cracking susceptibility. *Proceedings of 6th International Trends in Welding Research*, ed. S. A. David, pp. 609–614, ASM International.

18. Collins, M. G., Lippold, J. C., and Kikel, J. M. 2003. Quantifying ductility-dip cracking susceptibility in nickel-base weld metals using strain-to-fracture test. *Proceedings of 6th International Trends in Welding Research*, ed. S. A. David, pp. 586–590, ASM International.

19. Duvall, D. S., and Owczarski, W. A. 1967. Further heat-affected zone studies in heat-resistant nickel alloys. *Welding Journal* 46(9): 423-s to 432-s.

20. Cola, M. J., Hochanadel, P. W., Lewis, G. K., Lao, K., Vargas, V. D., and Kelly, A. M. 2003. Hot ductility testing of laser deposited alloy 690-initial studies. *Proceedings of 6th International Trends in Welding Research*, ed. S. A. David, pp. 591–596, ASM International.

21. Aoh, J. N., and Yang, C. H. 2003. Cracking susceptibility study of Inconel 600 alloy using Varestraint and hot ductility test. *Proceedings of 6th International Trends in Welding Research*, ed. S. A. David, pp. 597–602, ASM International.

22. Guo, H., Chaturvedi, M. C., and Richards, N. L. 2000. Effect of sulphur on hot ductility and heat affected zone micromicro-cracking in Inconel 718 welds. *Science and Technology of Welding and Joining* 5(6): 378–384.

23. Lippold, J. C. 1998. Recent advances in welding metallurgy. *Proc. Taiwan International Welding Conference*, pp. 35–46.

24. Qian, M., and Lippold, J. C. 2003. The effect of annealing twin-generated special grain boundaries on HAZ liquation cracking of nickel-base superalloys. *Acta Materialia* 51(2): 3351–3361.

25. Yang, J. G., and Qu, B. L. 2001. Hot ductility behavior and HAZ hot cracking susceptibility of 7475-T7351 aluminum alloy. *Scandinavian Journal of Metallurgy* 30(3): 146–157.

26. Ojo, O. A., and Chaturvedi, M. C. 2005. On the role of liquated γ′ precipitates in weld heat affected zone micro-cracking of a nickel-based superalloy. *Materials Science & Engineering A* 403 (1-2): 77–86.

27. Vekeman, I. J, and De Waele, I. M. Repair Welding of HP40-Nb. International Institute of Welding. *www.iiw-iis.org/iiw/extranet/static/MS/C-IX/C-IX-H/IX-2266-08_IX-H-673-08.pdf*

28. Penso, J. 2006. API committee round table discussion on standard of Refinery Equipment, Spring. *http://committees.api.org/standards/cre/sccm/meetings/docs/s06/repairmitmeadpenso.pdf.*

29. Davis, J. R. 1992. *ASM Materials Engineering Dictionary*. p. 174. ASM International.